Energy Storage Materials 67 (2024) 103291

Contents lists available at ScienceDirect

Energy Storage Materials

journal homepage: www.elsevier.com/locate/ensm

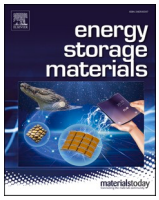

Stabilized high-voltage operation of Co-free NMX cathode via CEI-controlling

Myungeun Choi [a,b], Hyunbong Choi [c], Sangwoo Park [c], Won Mo Seong [c], Yongseok Lee [a,b], Wonseok Ko [a,b], Min-kyung Cho [d], Jinho Ahn [a,b], Youngsun Kong [c], Jongsoon Kim [a,b,*]

[a] Department of Energy Science, Sungkyunkwan University, Suwon, 16419, Republic of Korea
[b] SKKU Institute of Energy Science and Technology (SIEST), Sungkyunkwan University, Suwon 16419, Republic of Korea
[c] SDI R&D Center, Samsung SDI, Suwon, 16678, Gyeonggi-do, Republic of Korea
[d] Advanced Analysis Center, Korea Institute of Science and Technology (KIST), Seoul, 02792, Republic of Korea

ARTICLE INFO

Keywords:
Co-free $Li[Ni_{0.75}Mn_{0.25}]O_2$
High voltage
Electrolyte design
1,4-butane sultone
CEI
5.8 Ah prismatic cell

ABSTRACT

A current emerging trend in materials research for Li-ion batteries (LIBs) is exploring cathode materials whose price is neutral to global supply chain issues. In this regard, removing cobalt in conventional high-Ni $Li[Ni_xCo_yMn_z]O_2$ (NCM) cathodes has been adopted as one of the most promising strategies. However, Co-free $Li[Ni_xMn_y]O_2$ (NMX, $x < 0.8$, $y > 0.2$) cathodes should require the high voltage (≈4.5 V *vs.* Li/Li^+) operation to obtain the high energy density as the level of conventional high-Ni NCM cathodes, which is considered as the major barrier of their real application to the LIB industrial field. To address this issue, it is essential to develop the novel electrolyte system for optimizing the high voltage operation of NMX cathodes. In this study, a delicate consideration of the whole battery system's chemical ensemble and its target usage condition has been attempted, and, as an exemplifying example, a Co-free $Li[Ni_{0.75}Mn_{0.25}]O_2$ cathode has been paired to an conventional electrolyte with 1,4-butane sultone (BS) electrolyte additive. Since highest occupied molecular orbital (HOMO) energy of BS is lower than both other well-known electrolyte additives and similar with the carbonate-based solvent, BS enables formation of homogeneous and stable cathode-electrolyte interphase (CEI) layer especially at the high voltage (4.5 V *vs.* Li/Li^+). Thus, 1wt% BS-added electrolyte can result in excellent cyclability of the full cell based on a Co-free $Li[Ni_{0.75}Mn_{0.25}]O_2$ cathode even in the 5.8 Ah prismatic cell with ~78% capacity retention for 1000 cycles, which indicates that a Co-free $Li[Ni_{0.75}Mn_{0.25}]O_2$ cathode with BS-based electrolyte can be applied to the real LIB industry as the low-cost alternative to conventional high-Ni NCM cathodes.

1. Introduction

The forthcoming energy paradigm shift in mobilities, boosted by globally spreading decarbonization policies, is technically based on the evolutionary electrification of consumer vehicles [1,2]. The driving range of state-of-the-art electric vehicles (EVs) nearly approaches that of conventional engine-driven vehicles, which has been enabled by the introduction of high-energy-density Li-ion batteries (LIBs) [3]. Moreover, not only in terms of energy, but also in a viewpoint of affordability of current LIBs, the latest EVs have proven themselves as even stronger competitive than ever to its conventional counterparts [4]. From a cell-level perspective, this rapid advance in battery technology has mainly been based on thorough understanding of materials science. For example, the successful adoption of high-Ni (Ni ≥ 0.8 mol) $Li[Ni_xCo_yMn_z]O_2$, (NCM)) has contributed to developing EVs with superior driving range. The most recent version of commercial high-Ni NCM cathodes showed >800 Wh kg^{-1} [5]. However, recent sustained increases in raw material prices, particularly for Co sources, due to various global supply chain issues, suggest that relying on conventional high-Ni NCM cathode materials may not be the most economically feasible strategy in the EV market [6,7]. Instead, making batteries whose price neutral to their external circumstances is becoming the strongest strategy [8,9].

Recently, Co-free layered-oxide cathodes, $Li[Ni_xMn_y]O_2$ (NMX), have great attention as the ultimate goal of current LIB system, satisfying ultra-low-cost and high-energy-density simultaneously [10–12]. To

* Corresponding author.
E-mail address: jongsoonkim@skku.edu (J. Kim).

https://doi.org/10.1016/j.ensm.2024.103291
Received 26 December 2023; Received in revised form 14 February 2024; Accepted 21 February 2024
Available online 22 February 2024

significantly reduce the production cost of LIBs, it is also essential to decrease the Ni contents in the NMX compared to the high-Ni NCM. However, the decrease of Ni contents results in lower available energy density of $Li[Ni_xMn_y]O_2$ ($x\langle$ 0.8, $y\rangle$ 0.2) in the same charge/discharge cut-off voltages than those of the high-Ni NCMs [13,14]. Thus, the high voltage (~4.5 V *vs.* Li/Li^+) operation should be required for $Li[Ni_{0.75}Mn_{0.25}]O_2$ to get the similar energy densities with the conventional high-Ni NCM cathodes. However, this high voltage requirement (~4.5 V *vs.* Li/Li^+) leads to the catastrophic cathode-electrolyte side reactions and severe structural changes in the layered structure, which prevent the real application of the $Li[Ni_{0.75}Mn_{0.25}]O_2$ cathode [15–17]. Moreover, the aggravated transition metal (TM) dissolution occurred at the high voltage charging process leads to the accumulation of TM-containing impurities on cathode and even anode by chemical cross-over effect [18–21]. The cathode itself also experiences the harmful surface reconstruction reaction related to the TM loss and densification, which leads to the rise in charge-transfer resistance between cathode and electrolyte [22–24]. Since commercial LIB cells contain only lean amount of electrolyte inside, consumption of electrolyte by vigorous side reaction during the high voltage operation should give rise to a rapid growth of cell resistance and sudden end-of-life (EOL) event [25,26]. In particular, these side reactions occurred at the high voltage regions are further accelerated at the high temperature [27–30]. Although various researches have been conducted to address the detrimental phenomena occurring at the cathode-electrolyte interphase (CEI) in the high-Ni NCM cathodes, it is difficult to apply the same method for the high-Ni NCM cathodes based on the 4.3 V (*vs.* Li/Li^+) charging process to the $Li[Ni_{0.75}Mn_{0.25}]O_2$ cathode requiring the charging cut-off voltage of 4.5 V (*vs.* Li/Li^+) [31–34]. An effective approach has not yet been proposed for the commercialization of low-cost Li-ion batteries (LIBs) based on $Li[Ni_{0.75}Mn_{0.25}]O_2$, which should ensure stable operation in the high voltage regions. Considering the unprecedented harsh conditions that cathodes need to endure, especially, it is not only important to focus on the electrode protection but also to take into account the entire chemical ensemble of the LIB system and its essential usage conditions to make $Li[Ni_{0.75}Mn_{0.25}]O_2$ competitive.

In this study, we demonstrated that $Li[Ni_{0.75}Mn_{0.25}]O_2$ can be stably operated even at extremely harsh operation conditions in the LIB full cell system, such as high voltage (~4.5 V *vs.* Li/Li^+), high delithiation (>210 mAh g^{-1}) and high temperature (45 °C), by development of novel electrolyte system. To prevent both too thick formation and instability of CEI layers at charging to 4.5 V (*vs.* Li/Li^+), we tried to discover the novel electrolyte additives with low highest occupied molecular orbital (HOMO) energy compared to other well-known electrolyte additive for 4.3 V charging process, using first principles calculation. It was confirmed the HOMO level of 1,4-butane sultone (BS) is not only lower than those of other electrolyte additives but also similar with those of the carbonate-based solvent. Thus, our newly designed electrolyte containing BS exhibited the best formation of the stable CEI layers for $Li[Ni_{0.75}Mn_{0.25}]O_2$ at the charging cut-off voltage of 4.5 V (*vs.* Li/Li^+) in the half cell system, which is clearly distinct from the conventional electrolyte system for 4.3 V charging process. As a result, the $Li[Ni_{0.75}Mn_{0.25}]O_2$‖graphite full cell using the carbonate-based electrolyte with 1 wt% BS additive showed superior electrochemical performances in the voltage range of 2.9–4.45 V at the high temperature of 45 °C. The full cell with BS additive delivered large capacity and energy density of ~217 mAh g^{-1} and ~827 Wh kg^{-1}, respectively. Furthermore, its capacity was retained to ~80 % after 200 cycles at 200 mA g^{-1}, which is much better than the full cell using the base electrolyte without BS that shows just capacity retention of ~68 % at the same conditions. Especially, the remarkably enhanced cycle-performance in 5.8 Ah prismatic cell by BS additive suggested that BS is one of the most important key factor for real industrial application of the low-cost $Li[Ni_{0.75}Mn_{0.25}]O_2$-based LIBs.

2. Experimental section

2.1. Preparation of electrolyte samples

1.2 M $LiPF_6$ in EC/EMC/DMC (2:4:4 vol%) was used as the base electrolyte. In an argon-filled glovebox, 1,4-butane sultone (BS, ≥99 %, Sigma-Aldrich) additive was added into the base electrolyte and stirred at 100 RPM and 60 °C for 60 h. After stirring, it was rested for 3 days to stabilization. Tetraethyl orthosilicate (TEOS, ≥99 %, Sigma-Aldrich) and Tris(trimethylsilyl)borate (TMSB, 99 %, Sigma-Aldrich) sample also prepared as same way with BS sample.

2.2. Electrochemical characterization

$Li[Ni_{0.75}Mn_{0.25}]O_2$ cathode active materials (CAM) were provided by Samsung SDI. For a typical example of preparing CAM in Samsung SDI, co-precipitated $(Ni_{0.75}Mn_{0.25})OH$ precursor was mixed thoroughly with LiOH with a stoichiometric ratio and annealed at 850 °C for 10 h under an O_2 atmosphere.

For fabrication of the $Li[Ni_{0.75}Mn_{0.25}]O_2$ electrode, $Li[Ni_{0.75}Mn_{0.25}]O_2$ cathodes powder, conductive carbon, and polyvinylidene fluoride (PVdF)-based binder were mixed in 96 : 2 : 2 wt ratio in anhydrous *N*-methyl-2-pyrrolidone (NMP) solvent. The $Li[Ni_{0.8}Co_{0.1}Mn_{0.1}]O_2$ electrode was also fabricated by mixing 85 wt% active material, 5 wt% super P carbon black, and 1 wt% PVdF in NMP solvent. The slurry was homogenized and applied onto an aluminum foil using the doctor-blade method, and then dried at 120 °C for approximately one hour. The resulting cathode electrodes had an areal loading level of 10.5 mg cm^{-2}.

For the half cell test, 2032-type coin cells were prepared using the $Li[Ni_{0.75}Mn_{0.25}]O_2$ and $Li[Ni_{0.8}Co_{0.1}Mn_{0.1}]O_2$ electrodes, Li metal as reference/counter electrodes, separator (conducted by Samsung SDI), and 1.2 M $LiPF_6$ in EC/EMC/DMC (2:4:4 vol%) electrolyte with the 1 wt % BS additive. They were assembled in an Ar-filled glove box (H_2O, O_2 < 0.1 ppm). Galvanostatic charge/discharge tests were performed at various current rates (300–1500 mA g^{-1}) in the voltage range of 3.0–4.5 V (*vs.* Li/Li^+) using a battery test system (WonATech WBCS3000).

For the full cell test, same conditions with half cells except graphite electrode as the reference/counter electrode and voltage range of 2.9–4.45 V. The graphite was fabricated with the graphite and cmc (sodium salt of carboxymethyl cellulose)/sbr (styrene-butadiene rubber) using the Cu foil. Finally, CR2032-type full cells were assembled with the $Li[Ni_{0.75}Mn_{0.25}]O_2$ cathode and graphite anode (capacity ratio of negative and positive electrodes of ~1.11) in an Ar-filled glove box.

For the 5.8 Ah prismatic cell test, the same conditions of 1.2 M $LiPF_6$ in EC/EMC/DMC (2:4:4 vol%) and 1wt% BS-added electrolytes used for the coin-cell tests were applied to the prismatic cell tests. The charge and discharge current densities were 100 and 200 mA g^{-1}, respectively, and its charging protocol was based on the constant current-constant voltage (CC—CV) with a cut-off current to 40 mA g^{-1}. The voltage range was maintained between 3.0 V and 4.4 V. Moreover, the charge/discharge was performed at 66 mA g^{-1} every 60 cycles in whole cycles for reference performance test (RPT) to assess standard capacity and DC-IR characteristics. DC-IR analyses were conducted by recharging the cell to 50 % state of charge and discharging it for 10 s at 200 mA g^{-1}. DC-IR was calculated from the voltage change over current (ΔV/I) during this brief interval.

2.3. Materials characterization

The crystal structures of $Li[Ni_{0.75}Mn_{0.25}]O_2$ were characterized using X-ray diffraction (XRD, PANalytical) with Mo Kα radiation (λ = 0.70932 Å). Structural data were collected over the 2θ range of 4.6°–34.3° with a step size of 0.01°. The XRD patterns' angles were transformed using Cu Kα radiation (λ = 1.54178 Å) to contrast with previous research. The FullProf Rietveld program was used to analyze the XRD data [35]. The *operando* XRD patterns were obtained to monitor structural change

during charge/discharge at current density of 30 mA g^{-1} within the voltage range 3.0–4.5 V (*vs.* Li/Li^+). *Operando* XRD patterns of Li[$Ni_{0.75}Mn_{0.25}$]O_2 were also measured using an X-ray diffractometer (XRD, PANalytical) in the 2θ range of 7.0°−33.0° with a step size 0.013°, which was also transformed using Cu Kα radiation (λ = 1.54178 Å).

The morphology and particle size of Li[$Ni_{0.75}Mn_{0.25}$]O_2 were determined using scanning electron microscopy (SEM; Hitachi SU-8010), operated at 15 keV. Before the measurement, each specimen was coated with Pt nanoparticles to enhance the conductivity.

The morphology and particle size of Li[$Ni_{0.75}Mn_{0.25}$]O_2 were also determined using transmission electron microscopy (TEM; JEOL JEM-F200), operated at 300 keV. Before the measurement, the Li[$Ni_{0.75}Mn_{0.25}$]O_2 powder was sonicated in ethanol, and droplets of the suspension were spread onto a carbon-coated Cu TEM grid. The specimen was dried at room temperature overnight to evaporate the ethanol.

2.4. Computational details

All the density functional theory (DFT) calculations were performed using Gaussian 16 software package [36]. For all the calculations, spin-unrestricted density functional theory (DFT) was performed based on the Becke–Lee–Yang–Parr (B3LYP) hybrid exchange–correlation functional [37–39] and the triple-zeta valence polarization (TZVP) basis set [40–42]. The calculated molecular structures of the additives and solvents were visualized using Avogadro software [43]. The EC/EMC/DMC (2:4:4 vol%) solvent was considered by applying a dielectric constant of 21.468, as used in previous studies [44–46].

3. Results and discussion

3.1. High cut-off voltage: more energy density, more challenges

We performed various analyses to verify the successful preparation of Li[$Ni_{0.75}Mn_{0.25}$]O_2. The detailed analysis processes were provided in Supplementary Note 1 (including Fig. S1–2). To compete with conventional high-Ni NCM cathodes, achieving an energy density of over ~800 Wh kg^{-1} is crucial for Li[$Ni_{0.75}Mn_{0.25}$]O_2 (Fig. 1**a**) [47–51]. However, in the typical voltage range of 3.0–4.3 V (*vs.* Li/Li^+), which is commonly applied to ensure stable cycling, the specific capacity and energy density of Li[$Ni_{0.75}Mn_{0.25}$]O_2 are only ~180.7 mAh g^{-1} and ~686 Wh kg^{-1}, respectively. To address this limitation, we decided to increase the charge cut-off voltage to 4.5 V (*vs.* Li/Li^+), which results in the specific capacity and energy density of Li[$Ni_{0.75}Mn_{0.25}$]O_2 reaching ~216.8 mAh g^{-1} and ~827 Wh kg^{-1}, respectively. However, this change poses a

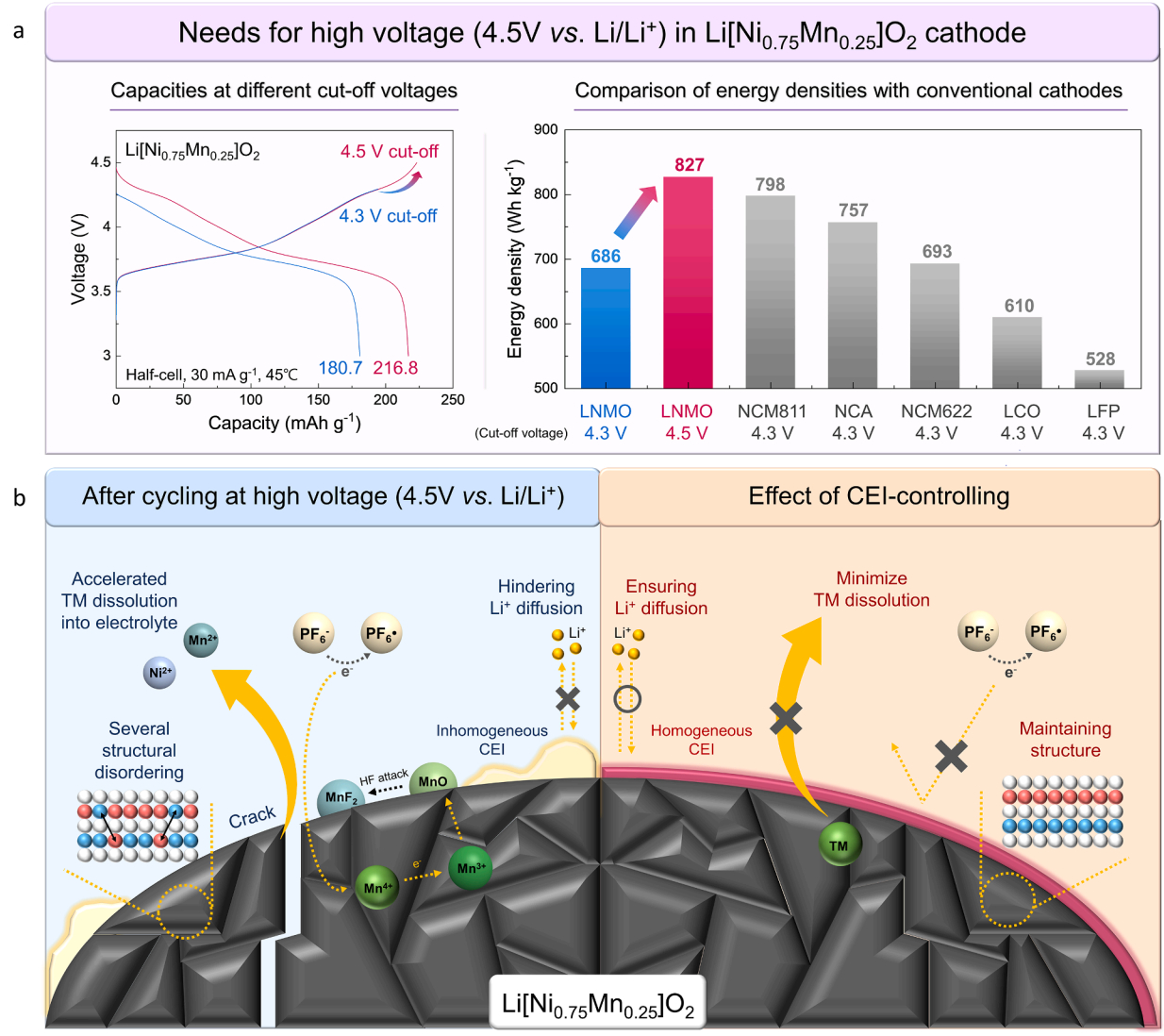

Fig. 1. Schematic image of (a) needs for high voltage in Li[$Ni_{0.75}Mn_{0.25}$]O_2 cathode. (b) Importance of stable and homogenous CEI formation for Li[$Ni_{0.75}Mn_{0.25}$]O_2 cathode requiring the high-voltage charging process.

new challenge, as maintaining performance for long-term cycling becomes difficult due to the side reactions from accelerated electrolyte decomposition at the high voltage of 4.5 V (Fig. 1**b**). It is also well-known that the hydrolysis of $LiPF_6$ in a battery cell leads to the formation of various acid compounds, including HF. This reaction occurs due to the high reactivity of $LiPF_6$ with even trace amounts of moisture present in the cell and especially accelerated at high voltage or temperature [52,53]. The HF compound attacks the well-established interfacial layer on the $Li[Ni_{0.75}Mn_{0.25}]O_2$ cathode. As a result, resistive LiF compounds are generated, which increase the resistance of the electrode and the internal pressure of the LIB. Additionally, HF causes the dissolution of TM ions from the cathode into the electrolyte, and it leads to the formation of resistive TM-based fluoride compounds on the cathode surface [54]. Finally, it contributes to several interfacial degradations, such as structural disordering or surface phase transitions, ultimately leading to the development of micro-cracks [55]. To make this promising $Li[Ni_{0.75}Mn_{0.25}]O_2$ cathode practical for commercial LIBs, a suitable electrolyte system must be designed to ensure stability even under harsh conditions involving high state of charge (SoC) and high voltage (4.5 V *vs.* Li/Li^+). Specifically, introducing small quantities of functional additives in the electrolyte can effectively safeguard the cathode electrode by forming a cathode-electrolyte interface (CEI) layer on the particles. The homogeneous CEI formed on electrode surface not only acts as a barrier against electrolyte side reactions at the cathode but also mitigates interfacial degradation caused by the irreversible phase transition of Ni-rich cathodes and the formation of micro-cracks within the secondary particle [56,57]. Thus, it is important to develop the optimal electrolyte system with the suitable additive to enable stable and outstanding electrochemical performances of $Li[Ni_{0.75}Mn_{0.25}]O_2$ even during charging to 4.5 V (*vs.* Li/Li^+).

3.2. *Development of the optimal electrolyte system for stable high voltage operation*

To explore the appropriate electrolyte additive for stable operation of $Li[Ni_{0.75}Mn_{0.25}]O_2$ at the high voltage region (4.5 V *vs.* Li/Li^+), we investigated the theoretical highest occupied molecular orbital (HOMO) and lowest unoccupied molecular orbital (LUMO) energy levels of the various additives and the carbonate-based solvents molecules using first-principles calculation. To prevent the formation of excessively thick CEI layers and instability during charging to 4.5 V (*vs.* Li/Li^+), the additive should have lower HOMO energy compared to the well-established additives applied for the stabilization during the 4.3 V charging process. Fig. 2a presented that the HOMO energy level of the BS additive is lower

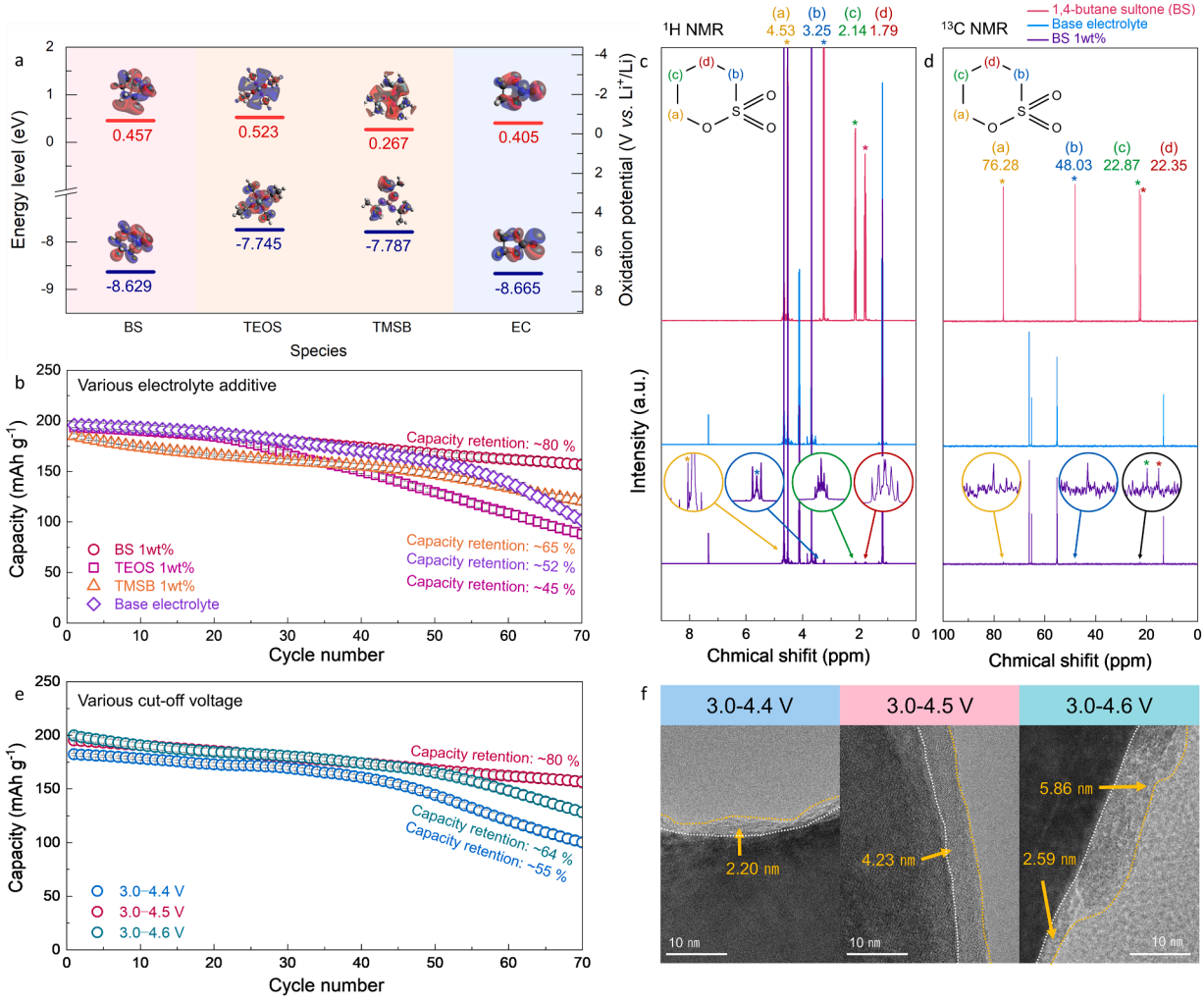

Fig. 2. (a) HOMO and LUMO energy levels of various additives and ethylene carbonate solvent. (b) Cycle performances of $Li[Ni_{0.75}Mn_{0.25}]O_2$ for 70 cycles at 200 mA g^{-1} using 1wt% of 1,4-butane sultone (BS), tetraethyl orthosilicate (TEOS) and Tris(trimethylsilyl)borate (TMSB) in base electrolyte with error bars displayed in insets. (c) ^1H, (d) ^{13}C NMR-spectra of the BS, base electrolyte and BS 1wt% electrolyte. (e) Cycle performances of $Li[Ni_{0.75}Mn_{0.25}]O_2$ for 70 cycles at 200 mA g^{-1} using BS 1wt% electrolyte at various cut-off voltages with error bars displayed in insets. (f) TEM images of $Li[Ni_{0.75}Mn_{0.25}]O_2$ electrodes after 70 cycles using BS 1wt % electrolyte at various cut-off voltages.

than other well-known additives such as tetraethyl orthosilicate (TEOS) or Tris(trimethylsilyl)borate (TMSB), furthermore, similar with the carbonate-based solvents. It implies BS can be participated in the reaction for CEI formation at the higher voltage region than other additives and can also initiate a reduction behavior shortly after the solvent decomposition. Specifically, the superoxide radical formed on the Ni-rich cathode surface during the charged state (> 4 V) triggers electrolyte oxidation through the dehydrogenation reaction of ethylene carbonate (EC) [58,59]. This leads to the production of gaseous products (CO_2 and CO) and harmful oligomers. Therefore, it is crucial that the additive begins decomposition shortly before the EC decomposition to mitigate undesirable outcomes.

Actually, the BS-applied electrolyte exhibited better cyclability in the voltage range of 3.0–4.5 V (*vs.* Li/Li^+) at 45 °C than not only base electrolyte (1.2 M $LiPF_6$ in EC:EMC:DMC=2:4:4 (v/v%)) but also the other-additive-added (1wt%) electrolytes (Fig. 2**b** and S3). Since we targeted to stable operation at the high voltage of 4.5 V, it becomes evident that BS is more suitable for $Li[Ni_{0.75}Mn_{0.25}]O_2$ compared to commonly used additives, considering their HOMO and LUMO energy level. To decouple the contribution of anode in the cycle lives, the capacity retention was re-measured up to 200 cycles with refreshment of Li metal and electrolytes every 40 cycles (Fig. S4). The periodic replenishment of a Li source contributed to the rise in initial discharge capacity every 40 cycles, and similar to above results, the sample with BS-applied electrolyte delivered enhanced cyclability. With the exception of anode, TEOS and TMSB additives showed insufficient stable CEI formation during cycling at high voltage, which was speculated to result in severe degradation of the cathode interfacial structure. Furthermore, electrochemical impedance spectra (EIS) analyses were performed to investigate the effect of BS additive on the electrode and electrolyte interfaces after cycling. As presented in Fig. S5, the introduction of 1wt% BS additive noticeably reduced the interfacial resistance in mid-frequency region after 70 cycles. Since charge-transfer resistances between two samples with base and 1wt% BS-added electrolytes were similar with each other, we speculated the main differences in the interfacial resistance originate from the CEI resistance. To further clarify the effect of BS on the surface, the X-ray photoelectron spectroscopy (XPS) S 2p spectra analyses was conducted. As shown in Fig. S6, it was demonstrated that decomposition products, such as Li_2SO_3 and $ROSO_2Li$, resulted from a series of reactions form the CEI layer on the surface of the Li $[Ni_{0.75}Mn_{0.25}]O_2$ electrode after 50 cycles. Based on the above results, it was verified that the BS additive was decomposed on the surface layer of $Li[Ni_{0.75}Mn_{0.25}]O_2$ and participated in the CEI formation. As the CEI forming additive, it is expected that BS would be decomposed via Li deintercalation at the cathode electrode in the Li cell system with possible reaction paths presented in Fig. S7. The initial stage of BS reduction involves the creation of a lithium ion-coordinated radical anion through a one-electron transfer (A). Subsequently, another electron transfer occurs, resulting in the formation of a radical alkyl sulfonate (B). Then, the radical alkyl sulfonate can yield various products, such as alkenyl sulfonate (C), alkyl sulfonate (D) and sulfonate dimers (E) [60]. According to the above results, it was speculated that the S═O functional group played an important role of facilitating the formation of the protective layer on the cathode during Li^+ extraction from cathode material, resulting in abundant formation of Li_2SO_3 and $ROSO_2Li$, main components of a stable CEI. [61–65] In addition, we performed ^1H and ^{13}C NMR analyses on BS, base electrolyte, and the 1wt% BS-added electrolyte (Fig. 2**c–d**). Although the peaks were weak due to the low contents, all the BS peaks were well-resolved at the similar chemical shift, which indicates successful preparation of the 1wt% BS-added electrolyte.

To validate the optimized cell condition with the 1wt% BS-added electrolyte, the cycle test was performed on a half cell with Li metal as anode, employing different voltage ranges and BS contents. All electrochemical tests were conducted at 45 °C to construct a more challenging environment, aimed at accelerating HF attack and the TM dissolution. To compare the electrochemical performances and CEI formation according to the cut-off voltage, we conducted the cycle tests on the BS sample with various cut-off voltages at 200 mA g^{-1} (Fig. 2**e-f** and S8). Interestingly, it was observed that the sample with a cut-off voltage of 4.4 V (*vs.* Li/Li^+) exhibited poorer capacity retention of ~55 % than the other samples. Moreover, as shown in the TEM images after 70 cycles, the formation of CEI layer to prevent HF attacks and TM dissolution during cycles was insufficient in the sample with a cut-off voltage of 4.4 V. This finding suggests that the BS additive is not suitable for the cut-off voltage condition below 4.4 V. In the case of the sample with the cut-off voltage of 4.6 V, the capacity retention was also lower than the sample with the cut-off voltage of 4.5 V and an excessively thick and uneven CEI layer was also detected. It implies that BS is not suitable for the typical 4.3 V cut-off voltage operation of NCM-based cathode materials, but rather specialized for Co-free $Li[Ni_xMn_y]O_2$ (NMX) cathodes requiring high-voltage operation above 4.5 V for obtaining high energy density as a level of high-Ni NCM, which is distinguished from the previous research on BS application for NCM111 [61]. In addition, the cycling performance was conducted with refreshment of Li metal and electrolyte every 40 cycles, solely to isolate the impact of anode on the cycle lives, employing different voltage ranges (Fig. S9). To further demonstrate the CEI formation process based on a cut-off voltage, the XPS S 2p spectra analyses were performed (Fig. S10). In contrast to the sample charged to 4.4 V with low intensity, the sample charged to 4.5 V exhibits increased intensity of Li_2SO_3 and $ROSO_2Li$, indicating sufficient formation of the CEI layer within the voltage range of 4.4 V to 4.5 V. Meanwhile, the sample charged to 4.6 V displayed higher intensity compared to the sample charged to 4.5 V, suggesting excessive decomposition of the BS, resulting in the formation of a thick CEI layer. Thus, compared to the other samples, the sample with a cut-off voltage of 4.5 V showed the best electrochemical performance and homogeneous formation of the CEI layer, which indicates that BS is suitable for the additive in the electrolyte for 4.5 V charging process. In addition, it was verified that the cycle retention of the samples with 0.5wt%, 1wt%, and 3wt% BS contents after 70 cycles at 200 mA g^{-1} in the voltage range of 3.0–4.5 V were ~55 %, ~80 %, and ~64 %, respectively (Fig. S11). Moreover, through comparison of TEM images among the samples, it was confirmed that the 1wt% BS-added electrolyte results in the well-formed and uniform CEI layer on the Li $[Ni_{0.75}Mn_{0.25}]O_2$ particles even after 70 cycles, which is clearly distinct from the 0.5wt% and 3wt% BS-added electrolyte displaying an excessively thin or thick and uneven CEI layers. These results indicate the optimized condition for $Li[Ni_{0.75}Mn_{0.25}]O_2$ electrode is the addition of 1wt% BS additive and the charging cut-off voltage of 4.5 V (*vs.* Li/Li^+).

3.3. *The effect of BS additive in the full cell system of $Li[Ni_{0.75}Mn_{0.25}]O_2$‖graphite*

To exclude the effect of Li metal and confirm the prospect in proposed electrolyte system, $Li[Ni_{0.75}Mn_{0.25}]O_2$ electrodes were investigated in full cell system employing graphite anode (Fig. 3**a-b**). As we changed the anode electrode from Li metal to graphite, we adjusted the voltage range to 2.9–4.45 V to minimize the hindrance of CEI formation caused by the BS additive. After the pre-cycle for 2 cycles, the samples using base and BS (1wt%)-added electrolytes exhibited the high specific capacities of ~217.3 and ~216.8 mAh g^{-1} at 30 mA g^{-1} (temperature: 45 °C), respectively. Interestingly, at a high current density of 1000 mA g^{-1}, the sample using the 1wt% BS-added electrolyte exhibited the specific capacity of ~154.5 mAh g^{-1}, whereas the sample using the base electrolyte just deliver a specific capacity of ~136.8 mAh g^{-1} at the same conditions. It is expected that the enhanced power-capability of the full cell in the high charging cut-off voltage of 4.45 V and the high temperature of 45 °C originates from the improved interfacial resistance through the application of BS in the electrolyte. Furthermore, the occurrence of the uniform redox reaction during charge/discharge processes at both cathode and anode interfaces with a sufficient N/P

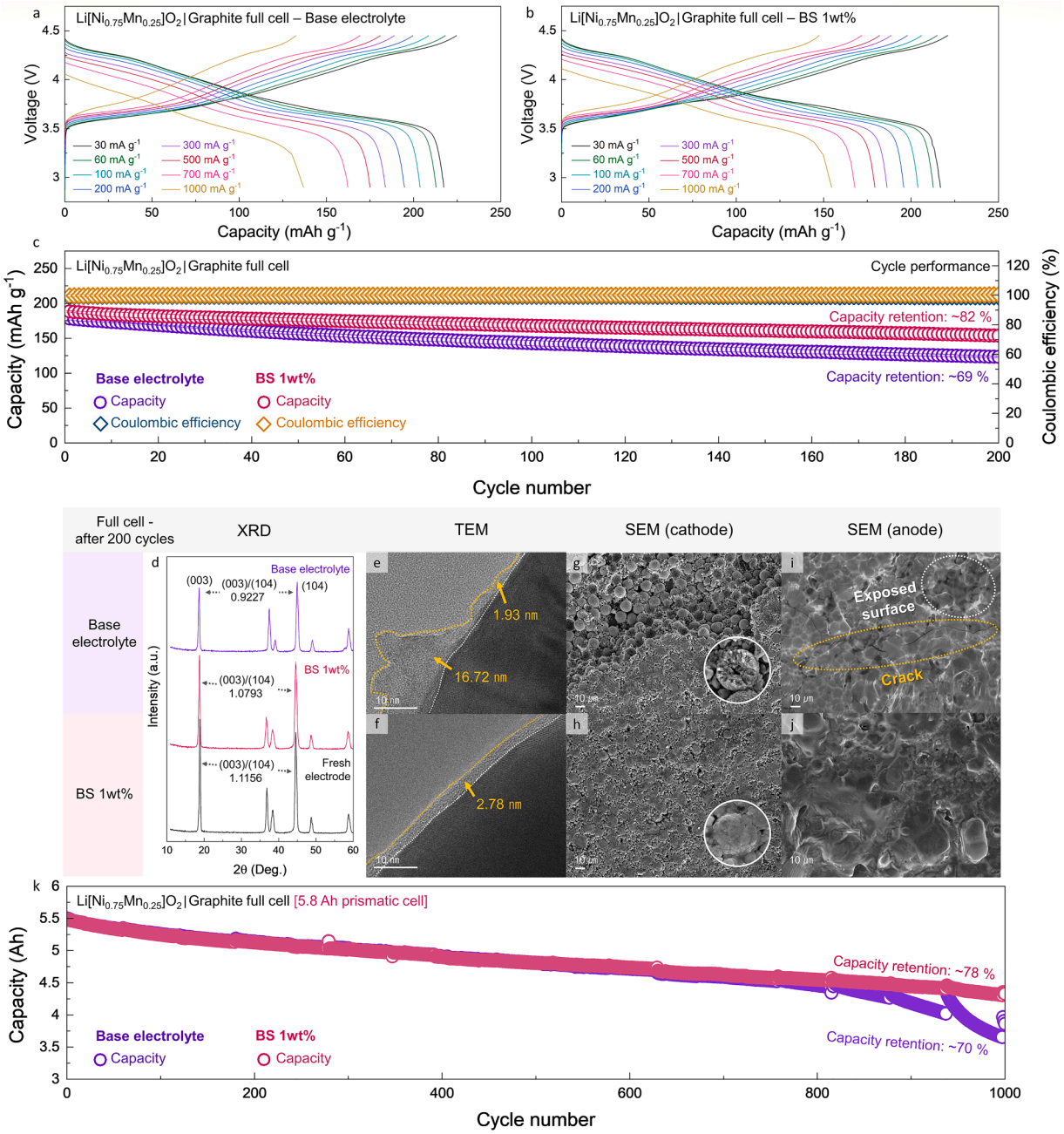

Fig. 3. Charge/discharge curves of $Li[Ni_{0.75}Mn_{0.25}]O_2$||graphite full cell using (a) base electrolyte, (b) 1wt% BS-added electrolyte in the voltage range of 3.0–4.5 V at various discharge current rates. (c) Cycle performances of $Li[Ni_{0.75}Mn_{0.25}]O_2$||graphite full cell for 200 cycles at 200 mA g^{-1} using base electrolyte and BS 1wt% electrolyte with error bars displayed in insets. (d) XRD patterns, (e, f) TEM images, (g, h) SEM images of $Li[Ni_{0.75}Mn_{0.25}]O_2$ electrodes and (i, j) SEM images of graphite electrodes after 200 cycles using base electrolyte and 1wt% BS-added electrolyte. (k) Cycle performance $Li[Ni_{0.75}Mn_{0.25}]O_2$|| graphite full cell in 5.8 Ah prismatic cell system.

ratio of 1.11 indicated that the cathode potential of the full-cell system could be attained around 4.5 V (Fig. S12) [66]. The tendency for securing the electrochemical stability through stable CEI formation was also verified in the cycling performance results. In Fig. 3**c** and S13, the cyclability of full cells demonstrated a significantly better performance compared to half cells, primarily attributed to being free from the degradation of Li metal, which occurs at a high temperature of 45 °C. After 200 cycles at 200 mA g^{-1} (45 °C), the sample using the 1wt% BS-added electrolyte exhibited the capacity retention of ~82 % compared to its initial capacity, while the sample using the base electrolyte only delivered a capacity retention of ~69 % compared with the initial capacity under the same conditions. Furthermore, it was demonstrated that the application of 1wt% BS could be helpful in improving interfacial resistance through EIS analyses using 200-cycled full cells (Fig. S14) tested in the high charging cut-off voltage and temperature. In the profiles of the EIS, both semicircles representing solid electrolyte interface resistance (R_{SEI}) and charge transfer resistance (R_{CT}) were significantly reduced in the sample using the 1wt% BS-added electrolyte, indicating that the protective BS-based CEI layer enhanced the interfacial stability of the electrode, leading to stable operation under the harsh conditions. In addition, to certify the effect of BS incorporation for universally applicable, we investigated the full cell test of $Li[Ni_{0.8}Co_{0.1}Mn_{0.1}]O_2$ (NCM811) cathode with 1wt% BS-added electrolyte. The discharge capacity of NCM811 cathode was delivered

to be approximately 200 mAh g^{-1} in the typical full-cell system [67,68]. As shown in Fig. S15 below, it was observed that the sample with BS additive exhibited capacity retention of ~79 % for 100 cycles, which is better than the sample without BS additive (~70 %). This result suggests that employing the BS-based electrolyte on Ni-rich layered oxide is generally effective in forming stable CEI mechanism.

Moreover, we conducted various analyses to investigate the successful protection of $Li[Ni_{0.75}Mn_{0.25}]O_2$ particles even in the harsh condition of the high charging cut-off voltage (4.45 V) and temperature (45 °C) by formation of stable CEI layer using the BS additive. As presented in Fig. 3d, it was observed that the sample using the base electrolyte is suffered from severe structural degradation compared to the sample using the 1wt% BS-added electrolytes. After cycling, the intensity of (003) peak was lower than that of (104) peak in the sample using the base electrolyte, whereas that in the sample using the 1wt% BS-added electrolyte was well retained. Considering that the ratio of (003)/(104) indicates with Li^+/Ni^{2+} cation mixing[69], these results indicate that a significant number of cations in the sample using the base electrolyte migrated from the TM layer to the Li layer after cycling, and BS additive can successfully protect the overall crystal structure of $Li[Ni_{0.75}Mn_{0.25}]O_2$. In addition, Fig. 3e reveals the presence of an inhomogeneous and uncontrolled CEI layer in the sample using the base electrolyte. The CEI layer exhibited significant thickness variation, ranging from ~16.72 nm to ~1.93 nm and this uneven thickness of the CEI layer contributes to the degradation of the cathode surface. On the other hand, the sample using BS 1wt% electrolyte exhibited formation of a robust and homogeneous CEI layer, protecting the electrode from degradation despite of the same conditions (Fig. 3f). Moreover, SEM analyses were performed on the cathode and anode electrodes of both samples using base and 1wt% BS-added electrolytes to evaluate the stability of the electrodes under repeated charge/discharge cycles according to the presence or absence of BS additives (Fig. 3g–j). After 200 cycles, the surface of the $Li[Ni_{0.75}Mn_{0.25}]O_2$ electrode using base electrolyte experienced complete surface destruction, leading to the exposure of the electrode's interior and even the fracturing of secondary particles. Similarly, that of graphite electrode also suffered several damage on surface and showed the critical cracks on particles. In contrast, both the $Li[Ni_{0.75}Mn_{0.25}]O_2$ and graphite electrodes using the 1wt% BS-added electrolyte exhibited a smooth and clean surface morphology, devoid of significant damage, resulting from the formation of a stable CEI layer. Furthermore, it was demonstrated that BS additive helped to suppress TM dissolution after long-time cycles compared to base electrolyte sample through SEM EDS-mapping using graphite electrodes after 200 cycles. (Fig. S16).

To further verify the effect of CEI-controlling in practical industrial systems, a $Li[Ni_{0.75}Mn_{0.25}]O_2$‖graphite full cell was tested in the 5.8 Ah prismatic cell system. The prismatic cell, with a capacity of 5.8 Ah, underwent 1000 charge-discharge cycles within the voltage range of 3.0–4.4 V. The cycling was conducted at the charge current density of 100 mA g^{-1} and the discharge current density of 200 mA g^{-1} and the CC—CV based charging protocol with a cut-off of 40 mA g^{-1} during charge. Moreover, DC-IR analyses were conducted by recharging the cell to 50 % SOC, then discharging it for 10 s at 200 mA g^{-1}. As shown in Fig. 3**k** and S17, the presence of BS contributed to stable long-term cycling, even at the high capacity of 5.8 Ah. In addition, the reference performance test (RPT) was performed with the charge/discharge current densities of 66 mA g^{-1} every 60 cycles up to 1000 cycles using the base and 1wt% BS-added electrolyte to assess standard capacity. It was verified that the degraded capacity of the prismatic cell using the base electrolyte was recovered after RPT and then sharply decayed in the afterward cycling. Furthermore, the full cell test on the coin cell system was conducted under identical electrochemical conditions to those of the prismatic cell system (Fig. S18). Consequently, both cycle-tests results of the coin and prismatic cell systems clearly showed the enhanced cyclability at the high charging cut-off voltage by application of 1wt% BS additive in the base electrolyte. DC-IR was calculated from the voltage change over current (ΔV/I) during this brief interval. Fig. S19 shows that 1wt% BS addition was found to have a positive influence on alleviating the internal resistance during long-term cycles. The prismatic cell using the base electrolyte showed a ΔDC-IR of 11.77 mΩ, while in the case of the prismatic cell using 1wt% BS-added electrolyte, this value was significantly lower at just 9.03 mΩ. Hence, these findings highlight the significant potential of BS as an electrolyte additive for the real industrial applications, facilitating stable operation at the high voltage for Co-free $Li[Ni_{0.75}Mn_{0.25}]O_2$.

3.4. *Suppressed structural degradation by application of BS additive*

Previous studies reported occurrence of the phase transition of the Ni-rich NCM cathode from the original hexagonal structure (H1) to the monoclinic phase (M), followed by the second hexagonal phase (H2) and the third hexagonal phase (H3) [15,70,71]. During initial delithiation process, the *c*-lattice parameter is enlarged owing to O—O repulsion. However, after further delithiation to high voltage region (4.5 V *vs.* Li/Li^+), the significant lattice shrinkage along the *c*-direction is occurred with phase transition to the H3-phase, which leads to volume changes and the accumulation of local stress, ultimately resulting in the formation and propagation of micro-cracks in secondary particles. In the case of $Li[Ni_{0.75}Mn_{0.25}]O_2$, the 4.5 V charging process is essential to get the high energy density, thus, it is very important to suppressed the severe structural degradation occurred during charge/discharge.

We conducted *operando* XRD analyses to understand the structural evolution of $Li[Ni_{0.75}Mn_{0.25}]O_2$ during charge/discharge and investigate how the BS additive suppress the structural degradation during charging to the high voltage region. The electrochemical tests for the *operando* XRD analyses was measured in the current density of 30 mA g^{-1} at 45 °C based on the half cell system. As shown in Fig. 4**a-b** and S20, the XRD patterns of the sample using the base electrolyte exhibited a noticeable shift that depended on the SoC. Specifically, the shift of the (003) reflection towards lower 2θ angles in the voltage range of 3.0 to 4.1 V (*vs.* Li^+/Li) indicates a progressive increase of the *c*-lattice parameter, which is associated with the H1-H2 phase transition in $Li[Ni_{0.75}Mn_{0.25}]O_2$. Subsequent delithiation occurred during charging from 4.1 V to 4.5 V caused a substantial contraction of the *c*-axis during the H2-H3 phase transition, resulting in a noticeable shift of the (003) reflection towards higher 2θ angles within contraction along the *c*-axis by ~2.6 %. Interestingly, the application of BS additive in the electrolyte provided highly enhanced structural stability of $Li[Ni_{0.75}Mn_{0.25}]O_2$ under same conditions (Fig. 4c-d). The sample using the 1wt% BS-added electrolyte delivered smaller shift of the maximum 2θ angle during the H2-H3 transition than that using the base electrolyte, despite of almost same specific capacities for both samples. The *c*-axis contraction in the sample using the 1wt% BS-added electrolyte during charging from 4.1 V to 4.5 V is just ~1.7 %, which is attributed to the stable protection of $Li[Ni_{0.75}Mn_{0.25}]O_2$ by the BS-based CEI layer. Moreover, it indicates that the stable formation of the CEI layer in the NMX cathode through BS application can result in not only suppression of the side reactions occurring at high voltages but also reduced lattice parameter variations and suppressed H2-H3 phase transition during charge/discharge, thereby inhibiting structural degradation of NMX cathode for prolonged cycling and improving the cycle-performance.

Furthermore, the dQ/dV analyses of $Li[Ni_{0.75}Mn_{0.25}]O_2$‖graphite full-cell depending on BS additive in the electrolyte supported the *operando* XRD results (Fig. S21a-b). Interestingly, the voltage regions at 3.6–3.9 V indicating the monoclinic phase were noticeably different for both samples using the based and 1wt% BS-added electrolytes. While the presence of the monoclinic phase was difficult to confirm in the dQ/dV curves when using the base electrolyte after 200 cycles, it was evident in the case of the 1wt% BS-added electrolyte even after 200th cycles. These findings suggest that $Li[Ni_{0.75}Mn_{0.25}]O_2$ using the base electrolyte undergoes the undesirable phase transition without the monoclinic phase due to the severe structural degradation during prolonged cycling with

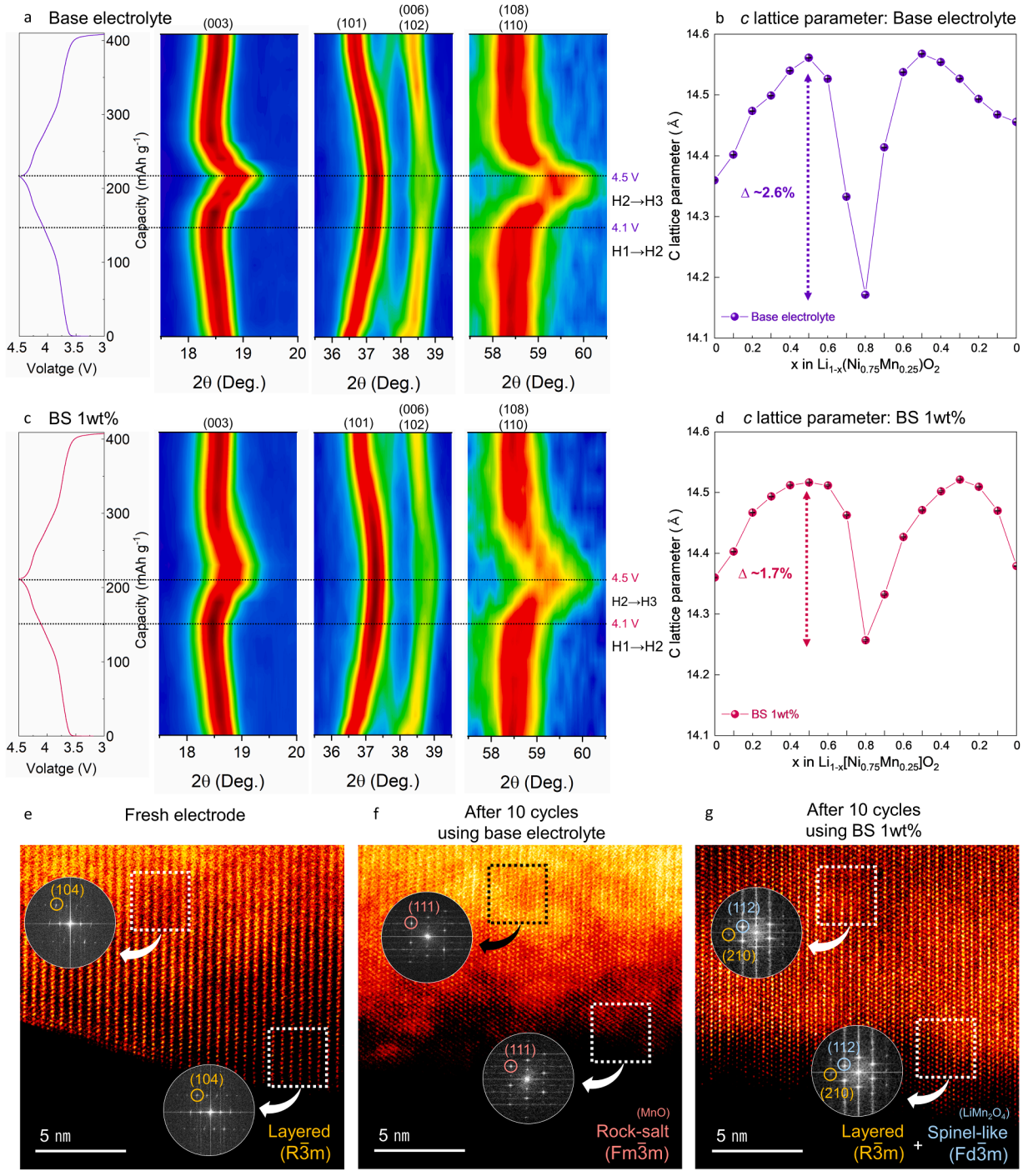

Fig. 4. *Operando/ex-situ* XRD patterns and change in lattice parameter *c* of $Li[Ni_{0.75}Mn_{0.25}]O_2$ using (a, b) base electrolyte, (c, d) 1wt% BS-added electrolyte during charge/discharge. HAADF-STEM images and FFT image of marked region of (a) fresh electrode and after 10 cycles using (f) base electrolyte, (g) 1wt% BS-added electrolyte.

the high charging cut-off voltage. In contrast, the application of BS additive allows for a stable and smooth phase transition during charge/discharge, including monoclinic phase even after 200th cycles, which results from the protection of $Li[Ni_{0.75}Mn_{0.25}]O_2$ structure by the stable BS-based CEI layer even in the high voltage region. As shown in Fig. S21c, it was observed that the proportion of the dQ/dV in the 4.1–4.45 V range for 200 cycles exhibited greater increase in the sample using the base electrolyte (+2.16 %) than that in the 1wt% BS-added electrolyte (+1.37 %). These results imply that H2-H3 phase transition during cycling was heavier occurred in the base electrolyte than the 1wt % BS-added electrolyte. Thus, we confirmed that the application of the BS additive effectively suppresses the H2-H3 transition of $Li[Ni_{0.75}Mn_{0.25}]O_2$ structure in the full cell even after charging to 4.45 V, leading to improving the structural stability during the prolonged cycling.

Additionally, we compared high-angle annular dark-field scanning transmission electron microscopy (HAADF-STEM) images between the samples using the base and 1wt% BS-added electrolytes after 10 cycles (Fig. 4e–g). In the case of the sample using the base electrolyte, it experienced severe structural degradation with formation of the rock-salt (Fm3̄m) phase in most of the surface region, which indicates that

the high structural instability of $Li[Ni_{0.75}Mn_{0.25}]O_2$ in the full cell during cycling in the harsh conditions (4.45 cut-off voltage and 45 °C operation). On the other hand, the sample using 1wt% BS-added electrolyte exhibited the relatively suppressed structural change of the surface to the mixed structure with layered and spinel-like ($Fd\bar{3}m$) phases, not the rock-salt phase at the same harsh conditions. These results also imply that TM dissolution in the surface of $Li[Ni_{0.75}Mn_{0.25}]O_2$ is effectively minimized through application of BS additive, which is also demonstrated using the *ex-situ* XPS analyses (Fig. S22–23). The formation of TM fluorides, such as MnF_2 and NiF_2, can serve as a direct indicator of TM dissolution. In the Mn and Ni $2p_{3/2}$ spectra, the sample using the base electrolyte sample exhibited higher peaks corresponding to MnF_2 (~642.1 eV) and NiF_2 (~858.3 eV), in comparison to that using the 1wt % BS-added electrolyte. These results suggest that the BS additive enables reduced TM dissolution due to the effective formation of a protective CEI layer in the harsh operation conditions for the Li $[Ni_{0.75}Mn_{0.25}]O_2$||graphite full cell.

4. Conclusion

In order to take advantage of the low-cost $Li[Ni_{0.75}Mn_{0.25}]O_2$ cathode, raising the cut-off voltage from 4.3 V to 4.5 V (*vs.* Li/Li^+) was crucial to compete with conventional cathodes in terms of energy density. However, the pursuit of higher energy density came with challenges, as the cell's vulnerability to instability at the high voltage by structural degradation. To address this challenge effectively, we proposed a strategy involving the introduction of an electrolyte additive, BS to promote the formation of homogeneous and stable CEI layer even at the high voltage, thereby enhancing the structural stability. Using first principles calculation and various experiments, it was confirmed that BS with lower HOMO energy than other well-known electrolyte additives enables the formation of the homogeneous and stable CEI layer on the surface of $Li[Ni_{0.75}Mn_{0.25}]O_2$ cathodes during charging to the high voltage. Moreover, we clearly demonstrated that the BS-based CEI layer effectively protected the $Li[Ni_{0.75}Mn_{0.25}]O_2$ cathode, preserving its crystal structure and particle morphology even in the high voltage charging process (to ≈4.5 V *vs.* Li/Li^+), using *operando* XRD, *ex-situ* HAADF STEM analyses, *etc*. These findings indicate that the application of the BS additive can help to stabilize the operation of the Li $[Ni_{0.75}Mn_{0.25}]O_2$-based full cell with high energy density in the high voltage condition, resulting in the highly enhanced cyclability and power-capability. Especially, in the 5.8 Ah prismatic cell system, BS-based electrolyte enables excellent cyclability with a capacity retention of ~78% for 1000 cycles, which is more outstanding than the base electrolyte. We believe this study provides valuable insights into understanding the compatibility between target usage conditions and the entire chemical landscape within a LIB cell when designing a cell that combines ultra-low cost, ultra-high energy density, and ultra-stable properties.

Declaration of competing interest

The authors declare that they have no known competing financial interests or personal relationships that could have appeared to influence the work reported in this paper.

CRediT authorship contribution statement

Myungeun Choi: Writing – original draft, Methodology, Investigation, Formal analysis, Data curation, Conceptualization. **Hyunbong Choi:** Validation, Resources, Investigation, Funding acquisition, Conceptualization. **Sangwoo Park:** Visualization, Validation, Resources, Conceptualization. **Won Mo Seong:** Resources, Investigation, Funding acquisition, Data curation, Conceptualization. **Yongseok Lee:** Validation, Methodology, Investigation. **Wonseok Ko:** Software, Methodology, Investigation, Data curation. **Min-kyung Cho:** Visualization, Software, Formal analysis. **Jinho Ahn:** Validation, Investigation, Conceptualization. **Youngsun Kong:** Resources, Project administration, Funding acquisition. **Jongsoon Kim:** Writing – review & editing, Supervision, Project administration, Investigation, Formal analysis, Data curation, Conceptualization.

Declaration of competing interest

The authors declare the following financial interests/personal relationships which may be considered as potential competing interests: Jongsoon Kim reports financial support was provided by Korea Institute of Science and Technology Information Seoul Office. Jongsoon Kim reports financial support was provided by Samsung SDI. If there are other authors, they declare that they have no known competing financial interests or personal relationships that could have appeared to influence the work reported in this paper.

Data availability

Data will be made available on request.

Acknowledgements

The financial support by Samsung SDI is gratefully acknowledged. The calculation resources were supported by the Supercomputing Center in Korea Institute of Science and Technology Information (KISTI) (KSC-2022-CRE-0415).

Supplementary materials

Supplementary material associated with this article can be found, in the online version, at doi:10.1016/j.ensm.2024.103291.

References

[1] G. Crabtree, The coming electric vehicle transformation: a future electric transportation market will depend on battery innovation, Science 366 (2019) 422–424.
[2] J. Bistline, N. Abhyankar, G. Blanford, L. Clarke, R. Fakhry, H. McJeon, J. Reilly, C. Roney, T. Wilson, M. Yuan, A. Zhao, Actions for reducing US emissions at least 50 % by 2030, Science 376 (2022) 923–924.
[3] C. Yang, Running battery electric vehicles with extended range: coupling cost and energy analysis, Appl. Energy 306 (2022) 118116.
[4] D. Castelvecchi, Electric cars and batteries: how will the world produce enough? Nature 596 (2021) 336–339.
[5] W. Li, E.M. Erickson, A. Manthiram, High-nickel layered oxide cathodes for lithium-based automotive batteries, Nat. Energy 5 (2020) 26–34.
[6] A. Zeng, W. Chen, K.D. Rasmussen, X. Zhu, M. Lundhaug, D.B. Müller, J. Tan, J. K. Keiding, L. Liu, T. Dai, A. Wang, G. Liu, Battery technology and recycling alone will not save the electric mobility transition from future cobalt shortages, Nat. Commun. 13 (2022) 1341.
[7] H. Wang, K. Feng, P. Wang, Y. Yang, L. Sun, F. Yang, W.-Q. Chen, Y. Zhang, J. Li, China's electric vehicle and climate ambitions jeopardized by surging critical material prices, Nat. Commun. 14 (2023) 1246.
[8] M. Fichtner, Recent research and progress in batteries for electric vehicles, Batter. Supercaps 5 (2022) e202100224.
[9] J.T. Frith, M.J. Lacey, U. Ulissi, A non-academic perspective on the future of lithium-based batteries, Nat. Commun. 14 (2023) 420.
[10] Y. Kim, W.M. Seong, A. Manthiram, Cobalt-free, high-nickel layered oxide cathodes for lithium-ion batteries: progress, challenges, and perspectives, Energy Storage Mater. 34 (2021) 250–259.
[11] G.-T. Park, B. Namkoong, S.-B. Kim, J. Liu, C.S. Yoon, Y.-K. Sun, Introducing high-valence elements into cobalt-free layered cathodes for practical lithium-ion batteries, Nat. Energy 7 (2022) 946–954.
[12] R. Zhang, C. Wang, P. Zou, R. Lin, L. Ma, L. Yin, T. Li, W. Xu, H. Jia, Q. Li, S. Sainio, K. Kisslinger, S.E. Trask, S.N. Ehrlich, Y. Yang, A.M. Kiss, M. Ge, B.J. Polzin, S. J. Lee, W. Xu, Y. Ren, H.L. Xin, Compositionally complex doping for zero-strain zero-cobalt layered cathodes, Nature 610 (2022) 67–73.
[13] L. de Biasi, B. Schwarz, T. Brezesinski, P. Hartmann, J. Janek, H. Ehrenberg, Chemical, structural, and electronic aspects of formation and degradation behavior on different length scales of Ni-rich NCM and Li-rich HE-NCM cathode materials in Li-ion batteries, Adv. Mater. (2019) 31.
[14] S.S. Zhang, Problems and their origins of Ni-rich layered oxide cathode materials, Energy Storage Mater. 24 (2020) 247–254.

[15] X. Fan, X. Ou, W. Zhao, Y. Liu, B. Zhang, J. Zhang, L. Zou, L. Seidl, Y. Li, G. Hu, C. Battaglia, Y. Yang, In situ inorganic conductive network formation in high-voltage single-crystal Ni-rich cathodes, Nat. Commun. 12 (2021) 5320.

[16] S. Jung, H. Gwon, J. Hong, K. Park, D. Seo, H. Kim, J. Hyun, W. Yang, K. Kang, Understanding the degradation mechanisms of $LiNi_{0.5}Co_{0.2}Mn_{0.3}O_2$ cathode material in lithium ion batteries, Adv. Energy Mater. 4 (2014) 1300787.

[17] X. Fan, G. Hu, B. Zhang, X. Ou, J. Zhang, W. Zhao, H. Jia, L. Zou, P. Li, Y. Yang, Crack-free single-crystalline Ni-rich layered NCM cathode enable superior cycling performance of lithium-ion batteries, Nano Energy 70 (2020) 104450.

[18] J. Betz, J. Brinkmann, R. Nölle, C. Lürenbaum, M. Kolek, M.C. Stan, M. Winter, T. Placke, Cross talk between transition metal cathode and Li metal anode: unraveling its influence on the deposition/dissolution behavior and morphology of lithium, Adv. Energy Mater. 9 (2019) 1900574.

[19] W. Liu, J. Li, W. Li, H. Xu, C. Zhang, X. Qiu, Inhibition of transition metals dissolution in cobalt-free cathode with ultrathin robust interphase in concentrated electrolyte, Nat. Commun. 11 (2020) 3629.

[20] Y. Li, W. Li, R. Shimizu, D. Cheng, H. Nguyen, J. Paulsen, S. Kumakura, M. Zhang, Y.S. Meng, Elucidating the effect of borate additive in high-voltage electrolyte for Li-rich layered oxide materials, Adv. Energy Mater. 12 (2022) 2103033.

[21] X. Zhang, Z. Cui, A. Manthiram, Insights into the crossover effects in cells with high-nickel layered oxide cathodes and silicon/graphite composite anodes, Adv. Energy Mater. 12 (2022) 2103611.

[22] T. Liu, L. Yu, J. Liu, J. Lu, X. Bi, A. Dai, M. Li, M. Li, Z. Hu, L. Ma, D. Luo, J. Zheng, T. Wu, Y. Ren, J. Wen, F. Pan, K. Amine, Understanding Co roles towards developing Co-free Ni-rich cathodes for rechargeable batteries, Nat. Energy 6 (2021) 277–286.

[23] M. Yi, W. Li, A. Manthiram, Delineating the roles of Mn, Al, and Co by comparing three layered oxide cathodes with the same nickel content of 70 % for lithium-ion batteries, Chem. Mater. 34 (2022) 629–642.

[24] A.V. Morozov, I.A. Moiseev, A.A. Savina, A.O. Boev, D.A. Aksyonov, L. Zhang, P. A. Morozova, V.A. Nikitina, E.M. Pazhetnov, E.J. Berg, S.S. Fedotov, J.M. Tarascon, E.V. Antipov, A.M. Abakumov, Retardation of structure densification by increasing covalency in Li-rich layered oxide positive electrodes for Li-ion batteries, Chem. Mater 34 (2022) 6779–6791.

[25] Q. Ma, X. Zhang, A. Wang, Y. Xia, X. Liu, J. Luo, Stabilizing solid electrolyte interphases on both anode and cathode for high areal capacity, high-voltage lithium metal batteries with high Li utilization and lean electrolyte, Adv. Funct. Mater. 30 (2020) 2002824.

[26] D. Peralta, J. Salomon, Y. Reynier, J.F. Martin, E. De Vito, J.F. Colin, A. Boulineau, C. Bourbon, B. Amestoy, C. Tisseraud, R. Pellenc, J.L. Ferrandis, D. Bloch, S. Patoux, Influence of Al and F surface modifications on the sudden death effect of Si-Gr/$Li_{1.2}Ni_{0.2}Mn_{0.6}O_2$ Li-Ion cells, Electrochim. Acta 400 (2021) 139419.

[27] G. Xu, C. Pang, B. Chen, J. Ma, X. Wang, J. Chai, Q. Wang, W. An, X. Zhou, G. Cui, L. Chen, Prescribing functional additives for treating the poor performances of high-voltage (5 V-class) $LiNi_{0.5}Mn_{1.5}O_4$/MCMB Li-ion batteries, Adv. Energy Mater. 8 (2018) 1701398.

[28] J.-G. Han, M.-Y. Jeong, K. Kim, C. Park, C.H. Sung, D.W. Bak, K.H. Kim, K.-M. Jeong, N.-S. Choi, An electrolyte additive capable of scavenging HF and PF_5 enables fast charging of lithium-ion batteries in $LiPF_6$-based electrolytes, J. Power Sources 446 (2020) 227366.

[29] D. Hu, Q. Zhang, J. Tian, L. Chen, N. Li, Y. Su, L. Bao, Y. Lu, D. Cao, K. Yan, S. Chen, F. Wu, High-temperature storage deterioration mechanism of cylindrical 21700-type batteries using Ni-rich cathodes under different SOCs, ACS Appl. Mater. Interfaces 13 (2021) 6286–6297.

[30] H. Park, H. Park, K. Song, S.H. Song, S. Kang, K.H. Ko, D. Eum, Y. Jeon, J. Kim, W. M. Seong, H. Kim, J. Park, K. Kang, In situ multiscale probing of the synthesis of a Ni-rich layered oxide cathode reveals reaction heterogeneity driven by competing kinetic pathways, Nat. Chem. 146 (14) (2022) 614–622.

[31] F. Cheng, X. Zhang, Y. Qiu, J. Zhang, Y. Liu, P. Wei, M. Ou, S. Sun, Y. Xu, Q. Li, C. Fang, J. Han, Y. Huang, Tailoring electrolyte to enable high-rate and super-stable Ni-rich NCM cathode materials for Li-ion batteries, Nano Energy 88 (2021) 106301.

[32] J. Ahn, T. Yim, Ni-rich $LiNi_{0.8}Co_{0.1}Mn_{0.1}O_2$ oxide functionalized by allyl phenyl sulfone as high-performance cathode material for lithium-ion batteries, J. Alloys Compd. 867 (2021) 159153.

[33] Y. Zou, K. Zhou, G. Liu, N. Xu, X. Zhang, Y. Yang, J. Zhang, J. Zheng, Enhanced cycle life and rate capability of single-crystal, Ni-rich LiNi0.9Co0.05Mn0.05O2 enabled by 1,2,4-1 H-triazole additive, ACS Appl. Mater. Interfaces 13 (2021) 16427–16436.

[34] Y. Zheng, N. Xu, S. Chen, Y. Liao, G. Zhong, Z. Zhang, Y. Yang, Construction of a stable $LiNi_{0.8}Co_{0.1}Mn_{0.1}O_2$ (NCM811) cathode interface by a multifunctional organosilicon electrolyte additive, ACS Appl. Energy Mater 3 (2020) 2837–2845.

[35] J. Rodríguez-Carvajal, Recent advances in magnetic structure determination by neutron powder diffraction, Phys. B Condens. Matter 192 (1993) 55–69.

[36] M.J. Frisch, G.W. Trucks, H.B. Schlegel, G.E. Scuseria, M.a. Robb, J.R. Cheeseman, G. Scalmani, V. Barone, G.a. Petersson, H. Nakatsuji, X. Li, M. Caricato, a. V. Marenich, J. Bloino, B.G. Janesko, R. Gomperts, B. Mennucci, H.P. Hratchian, J. V. Ortiz, a.F. Izmaylov, J.L. Sonnenberg, F.Ding Williams, F. Lipparini, F. Egidi, J. Goings, B. Peng, A. Petrone, T. Henderson, D. Ranasinghe, V.G. Zakrzewski, J. Gao, N. Rega, G. Zheng, W. Liang, M. Hada, M. Ehara, K. Toyota, R. Fukuda, J. Hasegawa, M. Ishida, T. Nakajima, Y. Honda, O. Kitao, H. Nakai, T. Vreven, K. Throssell, J.a. Montgomery Jr, J.E. Peralta, F. Ogliaro, M.J. Bearpark, J.J. Heyd, E.N. Brothers, K.N. Kudin, V.N. Staroverov, T.a. Keith, R. Kobayashi, J. Normand, K. Raghavachari, a.P. Rendell, J.C. Burant, S.S. Iyengar, J. Tomasi, M. Cossi, J. M. Millam, M. Klene, C. Adamo, R. Cammi, J.W. Ochterski, R.L. Martin, K. Morokuma, O. Farkas, J.B. Foresman, D.J. Fox, Gaussian, Inc., Gaussian 16, Revision C.01, Gaussian, Inc., Wallin, 2016.

[37] P.J. Stephens, F.J. Devlin, C.F. Chabalowski, M.J. Frisch, Ab Initio calculation of vibrational absorption and circular dichroism spectra using density functional force fields, J. Phys. Chem. 98 (1994) 11623–11627.

[38] C. Lee, W. Yang, R.G. Parr, Development of the Colle-Salvetti correlation-energy formula into a functional of the electron density, Phys. Rev. B 37 (1988) 785–789.

[39] A.D. Becke, Density-functional thermochemistry. III. The role of exact exchange, J. Chem. Phys. 98 (1993) 5648–5652.

[40] A. Schäfer, C. Huber, R. Ahlrichs, Fully optimized contracted Gaussian basis sets of triple zeta valence quality for atoms Li to Kr, J. Chem. Phys. 100 (1994) 5829–5835.

[41] A. Schäfer, H. Horn, R. Ahlrichs, Fully optimized contracted Gaussian basis sets for atoms Li to Kr, J. Chem. Phys. 97 (1992) 2571–2577.

[42] B. Klaumünzer, D. Kröner, P. Saalfrank, (TD-)DFT calculation of vibrational and vibronic spectra of riboflavin in solution, J. Phys. Chem. B 114 (2010) 10826–10834.

[43] M.D. Hanwell, D.E. Curtis, D.C. Lonie, T. Vandermeerschd, E. Zurek, G. R. Hutchison, Avogadro: an advanced semantic chemical editor, visualization, and analysis platform, J. Cheminform. 4 (2012) 1–17.

[44] R.P. Seward, E.C. Vieira, The dielectric constants of ethylene carbonate and of solutions of ethylene carbonate in water, methanol, benzene and propylene carbonate, J. Phys. Chem. 62 (1958) 127–128.

[45] A.B. McEwen, S.F. McDevitt, V.R. Koch, Nonaqueous electrolytes for electrochemical capacitors: imidazolium cations and inorganic fluorides with organic carbonates, J. Electrochem. Soc. 144 (1997) L84–L86.

[46] D.S. Hall, J. Self, J.R. Dahn, Dielectric constants for quantum chemistry and Li-ion batteries: solvent blends of ethylene carbonate and ethyl methyl carbonate, J. Phys. Chem. C 119 (2015) 22322–22330.

[47] H. Wu, B. Tang, X. Du, J. Zhang, X. Yu, Y. Wang, J. Ma, Q. Zhou, J. Zhao, S. Dong, G. Xu, J. Zhang, H. Xu, G. Cui, L. Chen, LiDFOB initiated in situ polymerization of novel eutectic solution enables room-temperature solid lithium metal batteries, Adv. Sci. 7 (2020) 1–9.

[48] Y. Han, S. Heng, Y. Wang, Q. Qu, H. Zheng, Anchoring interfacial nickel cations on single-crystal $LiNi_{0.8}Co_{0.1}Mn_{0.1}O_2$ cathode surface via controllable electron transfer, ACS Energy Lett. 5 (2020) 2421–2433.

[49] R. Zhang, Z. Meng, X. Ma, M. Chen, B. Chen, Y. Zheng, Z. Yao, P. Vanaphuti, S. Bong, Z. Yang, Y. Wang, Understanding fundamental effects of Cu impurity in different forms for recovered $LiNi_{0.6}Co_{0.2}Mn_{0.2}O_2$ cathode materials, Nano Energy 78 (2020) 105214.

[50] J. Li, M. Liu, J. An, P. Tian, C. Tang, T. Jia, F.K. Butt, D. Yu, W. Bai, C. Cao, X. Feng, The synergism of nanoplates with habit-tuned crystal and substitution of cobalt with titanium in Ni-rich $LiNi_{0.80}Co_{0.15}Al_{0.05}O_2$ cathode for lithium-ion batteries, J. Alloys Compd. 829 (2020) 154555.

[51] M. Fan, Q. Meng, X. Chang, C. Gu, X. Meng, Y. Yin, H. Li, L. Wan, Y. Guo, In situ electrochemical regeneration of degraded $LiFePO_4$ electrode with functionalized prelithiation separator, Adv. Energy Mater 12 (2022) 2103630.

[52] O.K. Park, Y. Cho, S. Lee, H.-C. Yoo, H.-K. Song, J. Cho, Who will drive electric vehicles, olivine or spinel? Energy Environ. Sci. 4 (2011) 1621.

[53] J. Han, C. Hwang, S.H. Kim, C. Park, J. Kim, G.Y. Jung, K. Baek, S. Chae, S.J. Kang, J. Cho, S.K. Kwak, H. Song, N. Choi, An antiaging electrolyte additive for high-energy-density lithium-ion batteries, Adv. Energy Mater. 10 (2020) 2000563.

[54] M.W. Park, S. Park, N.S. Choi, Unanticipated mechanism of the trimethylsilyl motif in electrolyte additives on nickel-rich cathodes in lithium-ion batteries, ACS Appl. Mater. Interfaces 12 (2020) 43694–43704.

[55] K. Kim, H. Ma, S. Park, N.S. Choi, Electrolyte-additive-driven interfacial engineering for high-capacity electrodes in lithium-ion batteries: promise and challenges, ACS Energy Lett. 5 (2020) 1537–1553.

[56] J.G. Han, E. Hwang, Y. Kim, S. Park, K. Kim, D.H. Roh, M. Gu, S.H. Lee, T.H. Kwon, Y. Kim, N.S. Choi, B.S. Kim, Dual-functional electrolyte additives toward long-cycling lithium-ion batteries: ecofriendly designed carbonate derivatives, ACS Appl. Mater. Interfaces 12 (2020) 24479–24487.

[57] J.W. Park, D.H. Park, S. Go, D.-H. Nam, J. Oh, Y.-K. Han, H. Lee, Malonatophosphate as an SEI- and CEI-forming additive that outperforms malonatoborate for thermally robust lithium-ion batteries, Energy Storage Mater. 50 (2022) 75–85.

[58] F. Wu, J. Dong, L. Chen, L. Bao, N. Li, D. Cao, Y. Lu, R. Xue, N. Liu, L. Wei, Z. Wang, S. Chen, Y. Su, High-voltage and high-safety nickel-rich layered cathode enabled by a self-reconstructive cathode/electrolyte interphase layer, Energy Storage Mater. 41 (2021) 495–504.

[59] J. Han, K. Kim, Y. Lee, N. Choi, Scavenging materials to stabilize $LiPF_6$-containing carbonate-based electrolytes for Li-ion batteries, Adv. Mater. 31 (2019) 1804822.

[60] B. Tong, Z. Song, H. Wan, W. Feng, M. Armand, J. Liu, H. Zhang, Z. Zhou, Sulfur-containing compounds as electrolyte additives for lithium-ion batteries, InfoMat 3 (2021) 1364–1392.

[61] X. Yu, Y. Wang, H. Cai, C. Shang, Y. Liu, Q. Wang, Enhancing the stability of high-voltage lithium-ion battery by using sulfur-containing electrolyte additives, Ionics (Kiel) 25 (2019) 1447–1457.

[62] L. Zhang, X. Zuo, T. Zhu, W. Huang, X. Zhao, W. Lei, X. Dongming, J. Liu, X. Xiao, J. Nan, 1-(P-toluenesulfonyl)imidazole (PTSI) as the novel bifunctional electrolyte for LiCoO 2-based cells with improved performance at high voltage, J. Power Sources 491 (2021) 229596.

[63] L. Liu, W. Gao, Y. Cui, S. Chen, A bifunctional additive bi(4-flurorophenyl) sulfone for enhancing the stability and safety of nickel-rich cathode based cells, J. Alloys Compd. 820 (2020) 153069.

[64] X. Zhang, Q. Wu, X. Guan, F. Cao, C. Li, J. Xu, Lithium dendrite-free and fast-charging for high voltage nickel-rich lithium metal batteries enabled by bifunctional sulfone-containing electrolyte additives, J. Power Sources 452 (2020) 227833.
[65] P. Dong, D. Wang, Y. Yao, X. Li, Y. Zhang, J. Ru, T. Ren, Stabilizing interface layer of $LiNi_{0.5}Co_{0.2}Mn_{0.3}O_2$ cathode materials under high voltage using p-toluenesulfonyl isocyanate as film forming additive, J. Power Sources 344 (2017) 111–118.
[66] J.K. Park, Principles and applications of lithium secondary batteries, Princ. Appl. Lithium Second. Batter. (2012).
[67] J. Zhang, H. Zhang, S. Weng, R. Li, D. Lu, T. Deng, S. Zhang, L. Lv, J. Qi, X. Xiao, L. Fan, S. Geng, F. Wang, L. Chen, M. Noked, X. Wang, X. Fan, Multifunctional solvent molecule design enables high-voltage Li-ion batteries, Nat. Commun. 14 (2023) 2211.
[68] M. Fang, B. Du, X. Zhang, X. Dong, X. Yue, Z. Liang, An electrolyte with less space-occupying diluent at cathode inner helmholtz plane for stable 4.6 V lithium-ion batteries, Angew. Chemie 136 (2024) e202316839.
[69] T. Weigel, F. Schipper, E.M. Erickson, F.A. Susai, B. Markovsky, D. Aurbach, Structural and electrochemical aspects of $LiNi_{0.8}Co_{0.1}Mn_{0.1}O_2$ cathode materials doped by various cations, ACS Energy Lett. 4 (2019) 508–516.
[70] G.-L. Xu, Q. Liu, K.K.S. Lau, Y. Liu, X. Liu, H. Gao, X. Zhou, M. Zhuang, Y. Ren, J. Li, M. Shao, M. Ouyang, F. Pan, Z. Chen, K. Amine, G. Chen, Building ultraconformal protective layers on both secondary and primary particles of layered lithium transition metal oxide cathodes, Nat. Energy 4 (2019) 484–494.
[71] S. Jung, H. Kim, S.H. Song, S. Lee, J. Kim, K. Kang, Unveiling the role of transition-metal ions in the thermal degradation of layered Ni–Co–Mn cathodes for lithium rechargeable batteries, Adv. Funct. Mater. 32 (2022) 2108790.